PERGAMON

International Journal of Heat and Mass Transfer 43 (2000) 1449–1456

International Journal of HEAT and MASS TRANSFER

www.elsevier.com/locate/ijhmt

Buoyant heat transfer in a rotating cup-like cavity

Won Nyun Kim[a], Ho Sang Kwak[b], Jae Min Hyun[a,*]

[a]Department of Mechanical Engineering, Korea Advanced Institute of Science and Technology, Yusong-ku, Taejon 305-701, South Korea

[b]Supercomputer Center, Electronics and Telecommunications Research Institute, Ueun-dong, Yusong-Ku, Taejon 305-333, South Korea

Received 6 November 1998; received in revised form 11 June 1999

Abstract

A numerical study is made of buoyant flow and heat transfer in a vertically mounted cup-like cylinder which rotates steadily about the longitudinal axis. The temperature at the cylinder sidewall is lower than that of the surroundings. The relevant nondimensional parameters are identified. The governing Navier–Stokes equations, with the Boussinesq-fluid approximation, are solved numerically. The rotational Reynolds number Re is large, and the cylinder aspect ratio is $O(1)$. The three-component velocity and temperature fields are portrayed. When the base surface is insulated, for the Richardson number $Ri \geq O(1)$, the meridional flow weakens, the boundary layer-like character in the temperature field diminishes, and the azimuthal flow approaches that of a rigid-body rotation. When the base surface is transferring, the velocity fields are little altered from those of the insulated base, but appreciable differences are seen in the temperature fields. Physical explanations and rationalizations are offered on the basis of numerical results. Detailed profiles of local Nusselt numbers at the solid boundaries are provided. The trends are consistent with the physical reasonings.

Keywords: Buoyant convection; Rotating cavity; Heat transfer enhancement

1. Introduction

Consider an open-ended, vertically-mounted cylindrical container (radius R, height L), sketched in Fig. 1, which rotates steadily about its own axis at rotation rate Ω. Near the top opening of this vessel, the rotation induces a downward axial motion of fluid toward the base of the container from the surroundings. Because of the presence of the impenetrable base surface, the fluid flows in the radially-outward direction near the base, and it moves upward along the cylindrical sidewall toward the opening. Therefore, at a given height of the vessel, the fluid flow in the central region is directed downward, and only at large radii close to the sidewall the flow is upward [1–4]. These fluid motions are maintained entirely by the rotation of the cylinder, and the character of flow is determined by the rotational Reynolds number Re ($\equiv \rho_w \Omega R^2/\mu$) and the aspect ratio A ($\equiv L/R$), where ρ_w and μ denote the reference density and coefficient of viscosity, respectively.

As observed by Sparrow and Chaboki [5], this flow configuration is of interest from the standpoint of basic fluid dynamics research as well as engineering applications. It is noted that, for this class of forced-convection flow, the transport phenomena are not influenced by the thermally-generated processes.

In typical technological situations, the Reynolds

* Corresponding author. Tel.: +82-42-869-3012; fax: +82-42-869-3210.

E-mail address: jmhyun@cais.kaist.ac.kr (J.M. Hyun).

0017-9310/00/$ - see front matter
PII: S0017-9310(99)00222-7

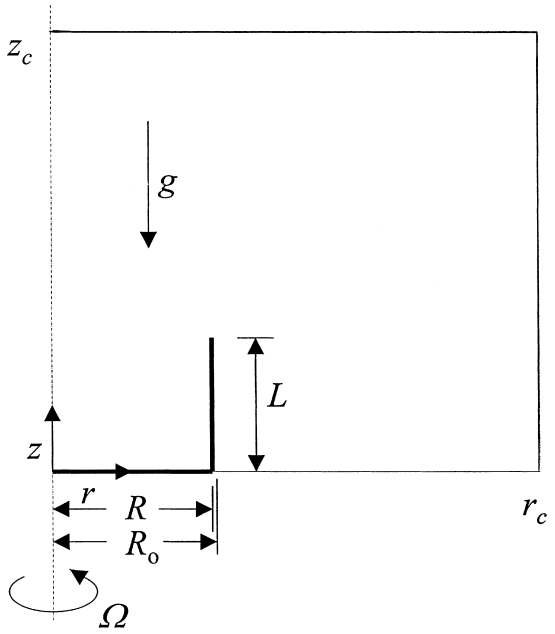

Fig. 1. Problem geometry and computation domain.

number Re is large and the aspect ratio $A \sim O(1)$. Sparrow and Chaboki [5], by invoking the analogy between heat and mass transfers, obtained experimentally the heat transfer coefficients by resorting to naphthalene sublimation techniques. Explicit dependencies of the surface-averaged Nusselt numbers at the cylindrical sidewall and at the base on Re, A and the Prandtl number Pr were presented for $600 \leq Re \leq 8000$. The above-stated experimental measurements of Sparrow and Chaboki [5] provided valuable data of the transport processes in the present forced-convection situations. Furthermore, physically insightful explanations and rationalizations were offered for the dynamical mechanisms involved. Recently, Kim and Hyun [1] and Kim et al. [2] acquired numerical solutions to the governing Navier–Stokes equations for the same flow geometry. These allowed detailed portrayals of flow and temperature fields over wider ranges of the relevant parameters. The behavior of the local and average Nusselt numbers at the boundary surfaces of the cylinder was described. The numerically-obtained average Nusselt numbers were in broad agreement with the earlier laboratory data of Sparrow and Chaboki [5] in the overlapping parameter range. These studies gave an overall picture delineating the principal flow and heat transfer features which are generated mechanically by the rotation of the cup-like cylindrical container.

In the present paper, the above configuration is recast to pose a mixed-convection problem by including the buoyancy effect. Specifically, the temperature T_w at the sidewall surface of the cylinder is lower than the temperature of the surroundings, T_∞. The key aspect here is that, near the vertical sidewall surface, the otherwise upward flow, which is driven by the rotation, is now opposed by the downward-directed buoyancy-induced current. Because of these competing dynamical elements, the entire meridional flow field is altered, which, in turn, gives rise to modifications in the azimuthal velocity. The temperature field, which is coupled to the flow field through buoyancy, and the attendant heat transfer in the cylinder undergo a fundamental readjustment [6]. The strength of buoyancy relative to the rotation effect will be gauged by the Richardson number Ri, and attention will be focused in the present study to the cases when these two effects are comparable, i.e., $Ri \sim O(1)$.

Comprehensive numerical solutions to the Navier–Stokes equations have been secured in the present effort, extending much of the procedures of preceding studies [1,2]. Flow and temperature fields are visualized in enlarged parameter ranges. In line with the original approaches of Sparrow and Chaboki [5], two types of thermal boundary conditions are considered for the base surface: in one case, the base surface is maintained to be adiabatic, which is referred to as type A; in the other case, both the base and cylindrical sidewall are at the same temperature, which is referred to as type B. The distributions of local Nusselt numbers as well as the surface-averaged Nusselt numbers are plotted as functions of the relevant flow parameters. Physical explanations are given to gain an understanding of the prominent dynamical ingredients and transport processes.

2. Numerical procedures

The Boussinesq-fluid approximation, $\rho = \rho_w[1 - \beta(T - T_w)]$, is invoked, in which β denotes the coefficient of thermometric expansion, and subscript w indicates the reference state at the cylindrical sidewall. The flow is governed by the steady, axisymmetric Navier–Stokes equations which, in properly-nondimensionalized standard notation, read

$$\frac{1}{r}\frac{\partial(ru^2)}{\partial r} + \frac{\partial(wu)}{\partial z} - \frac{v^2}{r} = -\frac{\partial p}{\partial r} + \frac{1}{Re}\left(\frac{1}{r}\frac{\partial}{\partial r}\left(r\frac{\partial u}{\partial r}\right) + \frac{\partial^2 u}{\partial z^2} - \frac{u}{r^2}\right) + \frac{Gr}{Re^2}\theta \quad (1)$$

$$\frac{1}{r}\frac{\partial(ruv)}{\partial r} + \frac{\partial(wv)}{\partial z} + \frac{uv}{r} = \frac{1}{Re}\left(\frac{1}{r}\frac{\partial}{\partial r}\left(r\frac{\partial v}{\partial r}\right) + \frac{\partial^2 v}{\partial z^2} - \frac{v}{r^2}\right) \quad (2)$$

$$\frac{1}{r}\frac{\partial(ruw)}{\partial r}+\frac{\partial(w^2)}{\partial z} = -\frac{\partial p}{\partial z}+\frac{1}{Re}\left(\frac{1}{r}\frac{\partial}{\partial r}\left(r\frac{\partial w}{\partial r}\right)+\frac{\partial^2 w}{\partial z^2}\right) \tag{3}$$

$$\frac{1}{r}\frac{\partial(ru)}{\partial r}+\frac{\partial w}{\partial z}=0 \tag{4}$$

$$\frac{1}{r}\frac{\partial(ru\theta)}{\partial r}+\frac{\partial(w\theta)}{\partial z}=\frac{1}{Re\cdot Pr}\left(\frac{1}{r}\frac{\partial}{\partial r}\left(r\frac{\partial\theta}{\partial r}\right)+\frac{\partial^2\theta}{\partial z^2}\right) \tag{5}$$

In the above, cylindrical coordinates (r, ϕ, z), with corresponding velocity components (u, v, w), are adopted. The thermophysical properties are taken to be constant. Here, R and $R\Omega$ were used as the length and velocity scale, respectively. The pertinent nondimensional parameters are the previously-defined Reynolds number Re, the Prandtl number Pr ($\equiv \mu/\alpha\rho_w$), the Grashof number Gr ($\equiv g\beta(T_\infty - T_w)R^3\rho_w^2/\mu^2$), in which α represents the thermal diffusivity and g the gravity. In Eq. (1), the parameter combination Gr/Re^2 is identified as the Richardson number Ri in mixed convection. The dimensionless temperature θ is defined as $\theta \equiv (T - T_w)/(T_\infty - T_w)$, in which $\Delta T[\equiv T_\infty - T_w] > 0$ in the present formulation.

In accordance with the problem statement, the fluid far from the cup is at rest and at constant temperature T_∞, i.e., $\theta = 1$. At the cylinder wall

$$u = w = 0, \quad v = 1 \quad \text{at } r = 1,\ 0 \le z \le L/R$$

$$u = w = 0, \quad v = r \quad \text{at } z = 0,\ 0 \le r \le 1 \tag{6}$$

As remarked in the introduction, the temperature conditions are, for type A (a non-transferring base):

$$\theta = 0, \quad \text{at } r = 1,\ 0 \le z \le L/R$$

$$\frac{\partial\theta}{\partial z} = 0 \quad \text{at } z = 0,\ 0 \le r \le 1; \tag{7a}$$

and for type B (the cylindrical sidewall and the base are at the same temperature)

$$\theta = 0, \quad \begin{cases} \text{at } r = 1,\ 0 \le z \le L/R \\ \text{at } z = 0,\ 0 \le r \le 1 \end{cases} \tag{7b}$$

The temperature at the outer surface (at $r = R_o$) of the cylindrical sidewall is assumed to be T_w,

$$u = w = 0, \quad v = R_o, \theta = 0 \quad \text{at } r = R_o/R,\ 0 \le z \le L/R \tag{8}$$

The above system of equations is solved by utilizing the well-documented numerical algorithm SIMPLER [7] and QUICK scheme [8] to handle convection terms. The highlights of the finite-volume schemes and solution methodologies have been widely publicized, and they are not reproduced here. As illustrated in Refs. [1,2], the calculation domain was taken to be sufficiently large to accommodate the main features of the earlier experiment [5]. The thickness of the solid cylindrical sidewall in the experiment [5] was not specified. In the present work, $R_o/R = 1.1$ was used. It is noted that the precise conditions at the outer surface of the sidewall have minimal impact on the global flow pattern inside the cup. Therefore, the exact value of R_o is of little concern here. As emphasized earlier, the transport process inside the cup is of concern, and the flow exterior to the cup is not of primary interest. The outer boundary of the computation domain was set at $r_c = 20.0$ and $z_c = 20.0$. A comprehensive check was made to establish the sensitivity of the results to the size of the domain. For several exemplary parameter sets, both r_c and z_c were varied between 10.0 and 100.0, and the corresponding changes in the computed flow variables inside the cup were typically less than 1%. In line with the previous approaches [1,2], at the domain boundaries,

$$\frac{\partial(ru)}{\partial r} = v = w = 0, \quad \theta = 1 \quad \text{at } r = r_c \tag{9}$$

$$u = v = \frac{\partial w}{\partial z} = 0, \quad \theta = 1 \quad \text{at } z = z_c \tag{10}$$

$$u = v = w = 0, \quad \theta = 1 \quad \text{at } z = 0,\ R_o/R \le r \le r_c \tag{11}$$

At the central axis, symmetry conditions are enforced [1,2]:

$$u = v = \frac{\partial w}{\partial r} = 0, \quad \frac{\partial\theta}{\partial r} = 0 \quad \text{at } r = 0 \tag{12}$$

For most calculations a staggered and stretched (100×100) mesh network was selected, with the grid points clustered near the solid boundaries. Progressively fewer grid points were placed at large radii and heights in the computational domain. Extensive convergence tests were performed of the computed results to grid spacing and stretching formula. Computations were repeated for several exemplary cases using (80×80), (100×100), (150×150) grids. The differences in the computed results were less than 1%. These exercises reinforced the adequacy and robustness of the present numerical model in grid-independence and accuracy.

3. Results and discussion

A series of numerical solutions were secured for the aspect ratio for A ($\equiv L/R$) = 1.0 and $Pr = 0.7$ for air. The rotational Reynolds number was set Re = 1000, and the Grashof number varied in the range $0 \le Gr \le 10^7$, which gave the Richardson number $0 \le Ri \le 10.0$.

First, the results for type A (a non-transferring base) are exhibited in Figs. 2–4. The plots of meridional stream function ψ, which is defined such that $u = (1/r)(\partial\psi/\partial z)$ and $w = -(1/r)(\partial\psi/\partial r)$, are displayed in Fig. 2. The result for $Gr = 0$, in Fig. 2(a) corresponds to the case of a non-buoyant flow, which was thoroughly examined in Refs. [1,2,5]. As described in Section 1, the rotation of the cup induces an axial flow toward the base, which is maintained by the celebrated pumping action of the Ekman layer at the base end-wall disk [9]. In the Ekman layer, the fluid is propelled radially-outward, and the flow turns into the axial direction toward the opening of the cup in the vicinity of the vertical sidewall. These overall features were portrayed by Kim and Hyun [1] and Sparrow and Chaboki [5], and Fig. 2(a) is corroborative of this qualitative flow pattern.

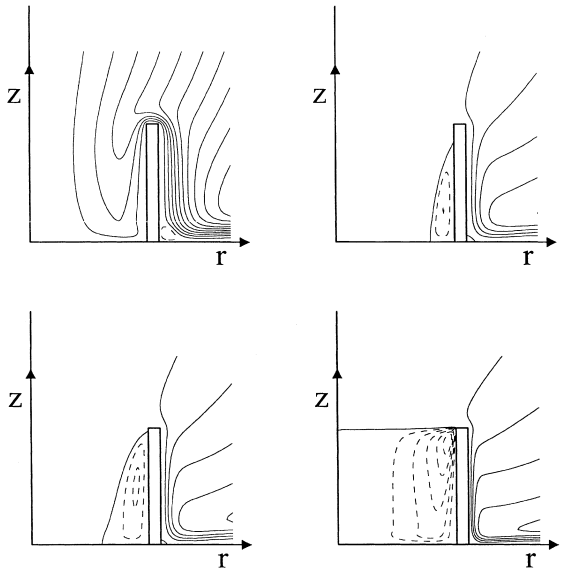

Fig. 2. Plots of meridional stream function ψ inside the cup. The base is insulated (type A). (a) $Ri = 0$, $\psi_{min} = 0$ and $\psi_{max} = 1.59 \times 10^{-2}$; the contour increment $\Delta\psi = 4.66 \times 10^{-3}$; (b) $Ri = 0.5$, $\psi_{min} = -7.2 \times 10^{-4}$ and $\psi_{max} = 3.4 \times 10^{-3}$ (when $\psi > 0$) and $\Delta\psi = 3.6 \times 10^{-4}$ (when $\psi < 0$); (c) $Ri = 1.0$, $\psi_{min} = -1.08 \times 10^{-3}$, and $\psi_{max} = 1.4 \times 10^{-3}$, $\Delta\psi = 1.4 \times 10^{-2}$ (when $\psi > 0$) and $\Delta\psi = 5.0 \times 10^{-4}$ (when $\psi < 0$); (d) $Ri = 10.0$, $\psi_{min} = -5.8 \times 10^{-3}$, and $\psi_{max} = 2.6 \times 10^{-4}$, $\Delta\psi = 2.4 \times 10^{-2}$ (when $\psi > 0$) and $\Delta\psi = 1.0 \times 10^{-3}$ (when $\psi < 0$) ; ψ_{min} and ψ_{max} are measured inside of the cup.

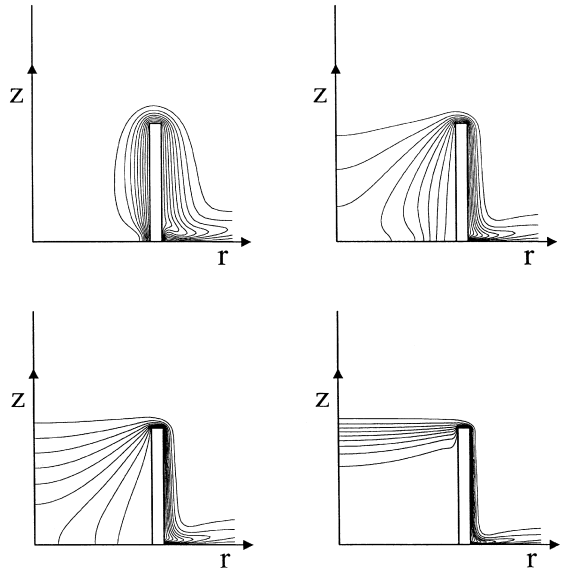

Fig. 3. Temperature fields. Type A. $\theta_{max} = 1.0$ and $\theta_{min} = 0.0$, and the contour increment $\Delta\theta = 0.1$. (a) $Ri = 0$; (b) $Ri = 0.5$; (c) $Ri = 1.0$; (d) $Ri = 10.0$.

For comparison purposes, consider a purely-buoyant flow in a non-rotating cup, with the temperature at the sidewall lower than that of the surroundings. The fluid

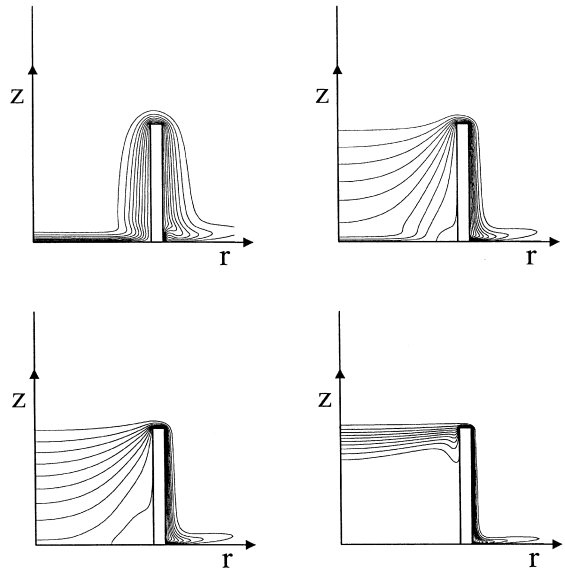

Fig. 4. Angular velocity v/r fields. Type A. $(v/r)_{max} = 1.0$ and $(v/r)_{min} = 0.0$, and the contour increment is 0.1. (a) $Ri = 0$; (b) $Ri = 0.5$; (c) $Ri = 1.0$; (d) $Ri = 10.0$.

in the immediate vicinity of the cold sidewall is cooled, and therefore, a sinking motion toward the base occurs [10], and it turns its direction radially-inward along the base, and, to conserve mass, the fluid moves out toward the opening in the central region. The general behavior of this buoyancy-driven meridional flow is opposite to that of the afore-stated rotation-induced flow pattern. Therefore, the relative strengths of these two competing dynamical elements, i.e., the effects of buoyancy and of rotation, are assessed by the Richardson number Ri ($\equiv Gr/Re^2$).

When the above two effects are comparable, much of the rotation-induced meridional flows are neutralized by the buoyancy effect, as is evident in Fig. 2(b) for $Ri = 0.5$. Only in the narrow region of close neighborhood of the sidewall, a weak clockwise, buoyancy-driven circulation is visible. As the buoyancy effect strengthens, the above trend becomes more distinct (see Fig. 2(c) for $Ri = 1.0$). Fig. 4(d) for $Ri = 10.0$ exemplifies the flow pattern which is dominated by the buoyancy effect, which illustrates a picture qualitatively opposite to the case of the purely rotation-induced flow of Fig. 2(a). It is worth pointing out that, when the buoyancy effect is dominant, the role of the boundary layer at the base is weak and passive in nature, in contrast to the active role played by the Ekman boundary layer in the rotation-dominant flow. Also, as demonstrated in Fig. 2(d), in the buoyancy-dominant case, the meridional flow is substantially confined to the interior region of the cup, and little fluid entrainment is seen between the surroundings and the interior of the cup. In passing, in the plots of the meridional stream function ψ in Fig. 2, the lines $\psi = 0$, separating the clockwise and counter-clockwise circulating cells, are shown inside of the cup. Furthermore, although it is not of direct interest here, a very small clockwise cell appears in the localized corner near the bottom of the exterior surface.

The temperature fields are exhibited in Fig. 3. In the case of non-buoyant flow, as shown in Fig. 3(a) for $Ri = 0$, concentration of isotherms near the sidewall is discernible. In the bulk of the interior, the temperature is mostly uniform at T_∞. Clearly, the augmentation of forced-convection heat transfer at the sidewall is obvious, and this is attributed to the enhanced meridional flows due to the Ekman layer pumping at the rotating base disk. When the buoyancy and rotation effects are comparable such that $Ri \sim O(1)$ (see Fig. 3(b) and (c)), the global temperature field loses the distinctive boundary layer-character near the sidewall, as demonstrated in Fig. 2(b) and (c). The overall strength of meridional flow is reduced, and, consequently, in the interior of the cup, the distribution of temperature is controlled primarily by conduction. These are reflected in more uniformly-spaced isotherms in the whole interior of the cup. When the buoyancy effect is dominant, the interior of the cup is substantially occupied by the buoyantly-controlled clockwise circulating flows which are initiated by the cold sidewall (see Fig. 2(d)). This brings forth a region of well-mixed fluid with temperature equalized to that of the sidewall T_w. In the vicinity of the height of the opening, the meridional flows are very weak, and conduction is the principal mode of heat transfer. In this region, the isotherms are mostly horizontal and vertically linearly-stratified from the well-mixed zone of the interior of the cup (T_w) to the surroundings (T_∞).

The behavior of angular velocity v/r inside the cup is revealing. For the non-buoyant case (see Fig. 4(a) for $Ri = 0$), at large radii near the sidewall, the boundary layer exists, and therefore, the angular velocity is largely uniform vertically and it decreases radially inward from the no-slip value of $v/r = 1.0$ at the sidewall. In the central portion of the interior of the cup, the angular velocity is negligibly small, implying that, in the bulk of the interior region, the fluid is almost non-rotating. This establishes the well-defined Ekman layer on the base in the central area up to moderate radii. The Ekman layer sucks in the fluid from the interior above into the boundary layer, and the magnitude of this Ekman pumping mechanism is proportional to $Re^{-1/2}$ and the difference in axial vorticity between the solid base and the fluid in the interior [9]. In the case of Fig. 4(a), the axial vorticity of the solid base is 2Ω (in dimensional terms) and that of the interior fluid is nearly zero. The axial suction of the interior fluid by the Ekman layer on the rotating base is the key ingredient to maintain the meridional flows in the interior of the cup. As the buoyancy effect becomes appreciable $Ri \sim O(1)$, the Ekman layer weakens, and the meridional flows caused by the Ekman suction are offset by the buoyancy-caused internal flows. Accordingly, the distribution of angular velocity v/r inside the cup decreases from the no-slip value of 1.0 at the solid-boundaries to very small values in the neighborhood of the opening of the cup (see Fig. 4(b) and (c)). When the buoyancy effect is dominant (see Fig. 4(d) for $Ri = 10.0$), the rotational effect represented by the Ekman suction virtually disappears. In much of the interior of the cup, therefore, the fluid is in rigid-body rotation with the angular velocity $v/r = 1.0$. In the narrow region in the vicinity of the opening of the cup, v/r undergoes a transition from the value of rigid-body rotation $v/r = 1.0$ to the stationary state in the surroundings ($v/r \rightarrow 0.0$).

Secondly, the results for type B, i.e., when the temperatures at the base and the sidewall are the same, are reviewed. The meridional flow patterns for type B are qualitatively similar to those for type A shown previously. This can be rationalized in the following way. For the non-buoyant case ($Ri = 0$), the meridional flow structure is determined mostly by the Ekman

pumping. Since the velocity and thermal fields are not coupled in this case, the precise form of thermal boundary condition at the base disk has little impact on the gross features of meridional flow. When the buoyancy effect is appreciable $Ri \sim O(1)$, the resulting meridional flow weakens substantially due to the buoyant flow induced by the cold sidewall. Therefore, the thermal condition at the base is immaterial. When the buoyancy effect is dominant ($Ri \geq O(1)$), the meridional flow in the interior of the cup is primarily controlled by the buoyancy-driven current at the sidewall. Consequently, the influence of the thermal condition on the base is of secondary importance. In summary, the change in the thermal condition at the base does not cause eminent alterations in the meridional flow characteristics. Similar arguments can be extended to the behavior of angular velocity field, i.e., the thermal boundary condition at the base exerts little influence on the determination of velocity fields in the interior of the cup.

As anticipated, however, the direct impact of thermal condition at the base is manifested in the temperature field. Comparison of Fig. 5 for type B with Fig. 3 for type A is useful. For the non-buoyant case ($Ri = 0$), a thermal boundary layer is discernible at the base, since the base is transferring (see Fig. 5(a)). This is in contrast to the case of non-transferring base (see Fig. 3(a)) in which such a thermal layer is absent. As the buoyancy effect becomes appreciable (see Fig. 5(b) and (c) for $Ri \sim O(1)$), the temperature field is more heavily influenced by conduction from the cold sidewall and base. Near the corner where the sidewall abuts the base, the zone of $\theta = 0$ is broader for type B than for type A, since both the sidewall and the base participate in the cooling of the fluid. When the buoyancy effect is dominant, the interior of the cup is influenced chiefly by the buoyancy-induced clockwise circulations. Accordingly, much of the interior is well-mixed, with its temperature determined principally by that of the sidewall. Consequently, in the limit of large Ri, the direct effect of the thermal boundary condition at the base is minor in the global temperature distributions in the interior.

Compiling the computed temperature data, the Nusselt numbers Nu at the boundary walls are defined such that

$$Nu_c = \left.\frac{\partial \theta}{\partial r}\right|_{r=1}, \quad \overline{Nu}_c = \int_0^{L/R} Nu_c \, dz,$$

and

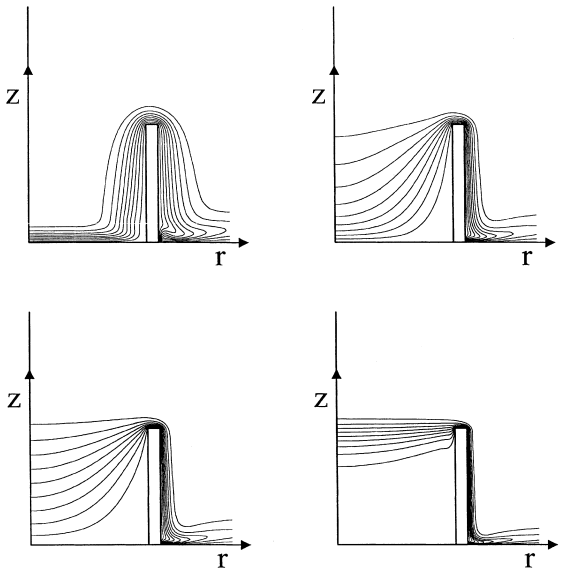

Fig. 5. Temperature fields. The base is transferring (type B). $\theta_{max} = 1.0$ and $\theta_{min} = 0.0$, and the contour increment $\Delta\theta = 0.1$. (a) $Ri = 0$; (b) $Ri = 0.5$; (c) $Ri = 1.0$; (d) $Ri = 10.0$.

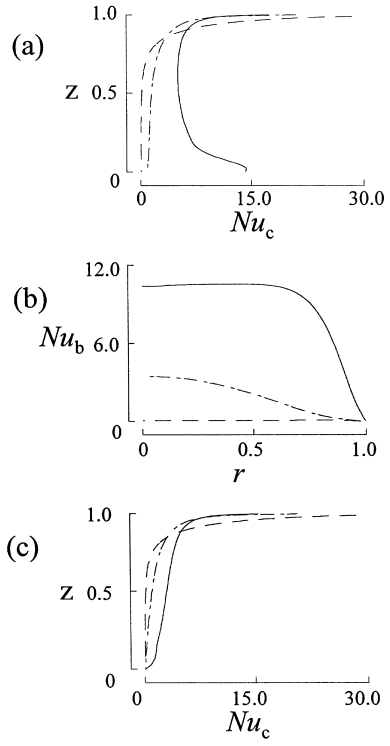

Fig. 6. Profiles of local Nusselt numbers. (a) Nu_c vs. z. Type A, (b) Nu_b vs. r. Type B, (c) Nu_c vs. z. Type B. —, $Ri = 0$; — —, $Ri = 0.5$; – · – $Ri = 10.0$.

$$Nu_b = \left.\frac{\partial\theta}{\partial z}\right|_{z=0}, \quad \overline{Nu}_b = 2\int_0^1 rNu_b\,dr,$$

in which is Nu_b meaningful only for type B, and subscripts c and b denote, respectively, the cylindrical sidewall and base. The overbar indicates the surface-averaged value.

Figs. 6 and 7 illustrate the behavior of local and average Nusselt numbers, respectively. When the relative strength of buoyancy effect is small (see $Ri \leq O(1)$), the flow is largely controlled by the rotation-induced Ekman pumping. For type A, the warm fluid in the surroundings is sucked into the cup toward the adiabatic base, and travels radially-outward near the base, and finally moves upward toward the opening along the cold sidewall, as depicted earlier. Since the base is non-transferring, the warm fluid maintains much of its temperature while flowing on the surface of the base. Heat transfer is vigorous, as the warm fluid washes along the surface of the cold sidewall, which turns up in large values of $\overline{Nu}_c$ for $Ri \leq O(1)$ type A. Qualitatively similar flow paths prevail for type B. However, the warm fluid from the surroundings undergoes heat transfer with the cold base while it flows radially-outward on the base surface, since the base is transferring. In other words, the fluid is precooled while moving along the surface of the base. Therefore, by the time this fluid flows upward along the sidewall, the difference in temperature between the pre-cooled fluid and the sidewall is smaller than for type A, which leads to reduced values of Nu_c for type B. The computed results of Nu_c and $\overline{Nu}_c$ illustrated in Fig. 6(a), (c) and 7(a) are consistent with this physical reasoning.

As the buoyancy effect becomes appreciable $Ri \sim O(1)$, the overall meridional flows diminish due to the comparable, but opposite, contributions by rotation-induced and buoyancy-induced motions. Consequently, the impact of the convective activities stemming from the meridional flows decreases in importance, and the Nu_c-values in general are reduced. Therefore, the precise form of thermal arrangement at the base becomes increasingly insignificant, and, accordingly, the gap between the values of Nu_c for type A and B narrows. These trends are reflected in Fig. 6(a), (c) and 7(a).

When the buoyancy effect is dominant $Ri > O(1)$, the heat transport inside the cup is carried out mostly by the buoyant current originating from the sidewall. The interior of the cup is occupied by buoyantly-controlled clockwise-circulating internal flows. The overall heat transfer coefficient Nu_c for $Ri > O(1)$ is slightly larger than the values obtainable for $Ri \sim O(1)$ when the convective activities are much subdued. Furthermore, in the buoyancy-dominated situations of $Ri > O(1)$, the exact thermal boundary condition at the base becomes irrelevant, since the global flow is shaped largely by the conditions at the sidewall.

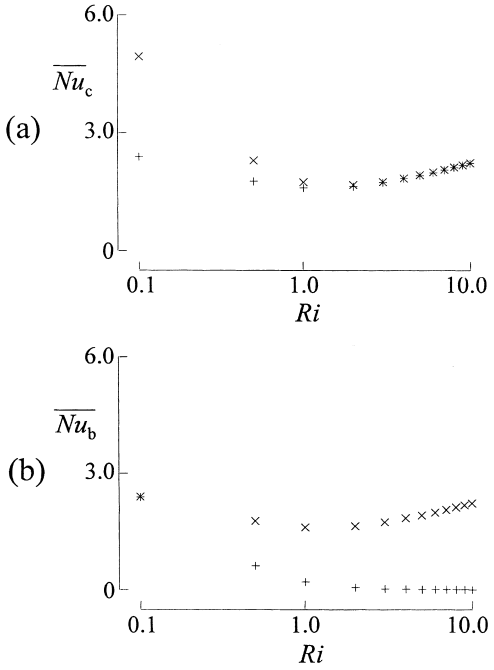

Fig. 7. Variations of $\overline{Nu}_c$. (a) $\overline{Nu}_c$ vs. Ri. x, type A; +, type B. (b) Type B. x, $\overline{Nu}_c$; +, $\overline{Nu}_b$.

4. Conclusion

For the case of the insulated base, as Ri increases, the weakening of meridional flows is evident. Concurrently, the temperature field in the interior of the cup changes its character from the boundary layer type for small Ri to the well-mixed uniform temperature for large Ri. The azimuthal-velocity field displays similar trends as Ri increases.

For the case of the transferring base, the global velocity pattern is qualitatively akin to the case of the insulated base. However, since heat transfer is allowed through the base, the temperature field exhibits appreciable departures from the case of the insulated base.

Detailed profiles of local Nusselt numbers at the boundaries are revealing. In general, the Nusselt number at the sidewall is higher for the case of the insulated base than for the transferring base. However, for large Ri, since the gross flow processes are controlled largely by the sidewall conditions, the difference in Nu_c diminishes between the two cases.

Acknowledgements

Appreciation is extended to the referee who provided detailed and constructive comments. This work was supported in part by the research grants from MOST, and KOSEF of Korea.

References

[1] W.N. Kim, J.M. Hyun, Mass transfer characteristics for a rotating cup-like cylinder, Int. J. Heat Mass Transfer 38 (1995) 2959–2967.
[2] W.N. Kim, J.M. Hyun, H. Ozoe, Effect of aspect ratio on mass transfer from a rotating cup, Int. J. Heat Mass Transfer 39 (1996) 2375–2377.
[3] S. Gilham, P.C. Ivey, J.M. Owen, J.R. Pincombe, Self-induced flow in a rotating tube, J. Fluid Mech 230 (1991) 505–524.
[4] S. Gilham, P.C. Ivey, J.M. Owen, Self-induced flow and heat transfer in a rotating tube, Int. J. Heat Fluid Flow 14 (1993) 27–36.
[5] E.M. Sparrow, A. Chaboki, Heat transfer coefficients for a cup-like cavity rotating about its own axis, Int. J. Heat Mass Transfer 25 (1982) 1333–1341.
[6] W.N. Kim, J.M. Hyun, Convective heat transfer in a cylinder with a rotating lid under stable stratification, Int J. Heat Fluid Flow 18 (1997) 384–388.
[7] S.V. Patankar, Numerical Heat Transfer and Fluid Flow, Hemisphere/McGraw-Hill, New York, 1980.
[8] T. Hayase, J.A.C. Humphrey, R. Grief, A consistently formulated QUICK scheme for fast and stable convergence using finite-volume iterative calculation procedures, J. Comput. Phy 98 (1994) 108–118.
[9] H.P. Greenspan, The Theory of Rotating Fluid, Cambridge University Press, Cambridge, 1968.
[10] A. Bejan, Convection Heat Transfer, 2nd ed., Wiley, New York, 1995.